



Seasonal predictability of the Atlantic Warm Pool in the NCEP CFS

Vasubandhu Misra^{1,2} and Steven Chan²

Received 24 June 2009; accepted 27 July 2009; published 27 August 2009.

[1] The July–August–September (JAS) seasonal predictability of the Atlantic Warm Pool (AWP) is examined in the extensive set of seasonal hindcasts of the National Centers for Environmental Prediction (NCEP) Climate Forecast System (CFS). We conduct both deterministic and probabilistic skill analyses of the NCEP CFS Seasonal Hindcasts (SHs). This study reveals that the SHs have a reasonable climatology of the AWP. The presence of robust decadal variability in sea surface temperature (SST) observations, while absent in the SHs, does seem to indicate its influence on the seasonal errors of the AWP in the NCEP CFS. However, after filtering out the observed SST for variability greater than 8 years, there is no systematic relation of AWP seasonal errors in the NCEP CFS with lead time. The signal to noise ratio of the area of the AWP in the SHs decreases with lead time, largely due to increases in the ensemble spread (noise). It is sobering to note that there is barely any probabilistic skill in the NCEP CFS SHs for the prediction of the anomalous AWP events (occurring either in the upper or lower terciles) at nearly all lead times. However if we examine the SHs from 1981–1996, when the observed SST in the AWP region is in one uniform phase of the prevalent decadal variation, then the SHs display useful skill in the prediction of anomalously large AWP events at all lead times. Furthermore, these truncated SHs also show significant probabilistic skill in the prediction of small (lower tercile) and normal (middle tercile) AWP events up to a lead time of 1 month. **Citation:** Misra, V., and S. Chan (2009), Seasonal predictability of the Atlantic Warm Pool in the NCEP CFS, *Geophys. Res. Lett.*, 36, L16708, doi:10.1029/2009GL039762.

1. Introduction

[2] The Atlantic Warm Pool (AWP), as the name suggests is a region of warm sea surface temperature (SST) that appears in the boreal summer and fall season in the Gulf of Mexico, the Caribbean Sea region, and over the western tropical Atlantic Ocean [Wang and Enfield, 2001]. The AWP has received growing attention with the detection of its possible influence on the interannual variations of summertime precipitation over the Great Plains, the Caribbean region, Mexico, and Central America [Wang *et al.*, 2008a, 2006; Wang and Enfield, 2003, 2001]. The relationship between the AWP area variability and Atlantic tropical cyclone activity is also well documented [Wang *et al.*, 2008b, 2006]. The AWP therefore offers a potential source

of seasonal predictability in the western hemisphere during the boreal summer season [Wang and Enfield, 2003; Wang *et al.*, 2006]. It is a well-known fact that the boreal summer season precipitation variability and predictability is a very challenging problem [Kang *et al.*, 2004]. In addition, it appears that the interannual variation of the AWP area is independent of El Niño Southern Oscillation (ENSO) variability in the eastern Pacific Ocean [Wang *et al.*, 2006]. This feature also encourages exploration of the AWP as a potential independent source of boreal summer season predictability in the western hemisphere.

[3] This study is aimed at understanding the seasonal predictability of the AWP in coupled-ocean atmosphere climate forecast systems. The National Centers for Environmental Prediction (NCEP) has provided the community with an extensive set of seasonal hindcasts from its Climate Forecast System (CFS) [Saha *et al.*, 2006], which provides an ideal opportunity to investigate the predictability of the AWP. Misra *et al.* [2009] showed that the NCEP CFS has a reasonable climatology of the AWP. In contrast, many of the Intergovernmental Panel on Climate Change Fourth Assessment Report (IPCC AR4) models was found to have some significant cold bias in the AWP region, which made even defining the AWP difficult [Misra *et al.*, 2009]. Given that the NCEP CFS is the US operational dynamical climate forecast system and is able to simulate the AWP, it is pertinent to examine whether there is skill in the NCEP CFS in predicting anomalous AWP events, whether initialization errors are grave to AWP prediction, and how the predictability of the AWP changes with lead time.

2. Data

[4] The NCEP CFS hindcast dataset is an extensive set of seasonal hindcasts (SHs) [Saha *et al.*, 2006]. In this study we used 23 years of data covering the period between 1981 and 2003. A SH consists of 15 ensemble members (readers are referred to Saha *et al.* [2006] for details on how they are generated), which are launched in the beginning of each month of the year. The length of each SH is 9 months. We specifically examine the SHs that start in the months of January, February, March, April, May, June, and July, because the AWP matures in the July–August–September (JAS) season [Wang and Enfield, 2001]. These SHs correspond to lead times of 6, 5, 4, 3, 2, 1, and 0 month for the JAS season. We also make use of the long-term NCEP CFS integrations that consist of 4 ensemble members, each integrated to a period of 32 years (hereinafter referred as LT; a brief outline of this integration is available in the auxiliary material).³ For observations, we use the NOAA Extended Reynolds SST version 3 following Smith *et al.*

¹Department of Meteorology, Florida State University, Tallahassee, Florida, USA.

²Center for Ocean-Atmospheric Prediction Studies, Florida State University, Tallahassee, Florida, USA.

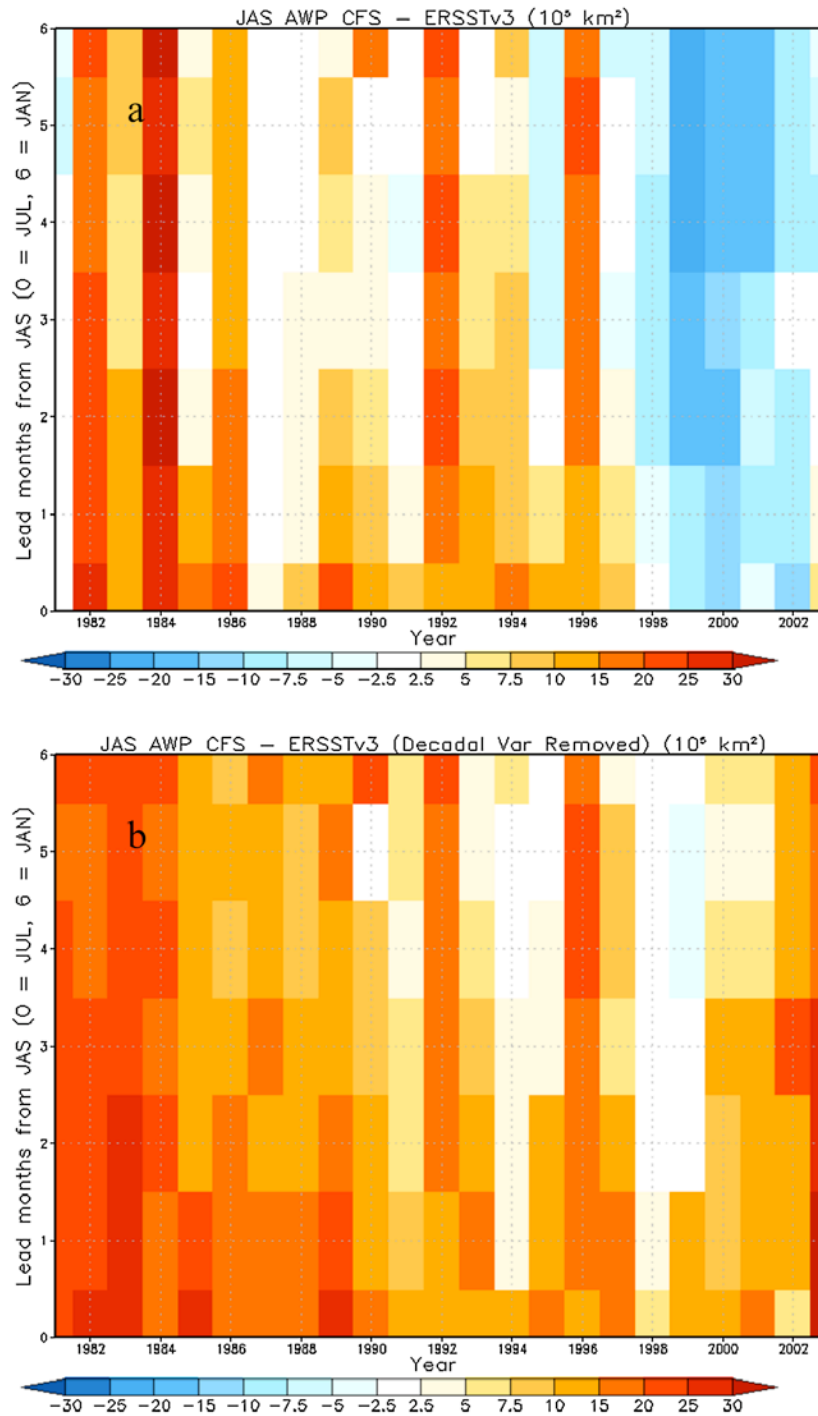


Figure 1. The JAS seasonal mean errors of the AWP computed relative to (a) observed SST and (b) high pass filtered observed SST, to remove variability greater than 8 years.

[2008]. When we compare SH with observations, then we match the observation period with the SH. But in comparing with the LT integration we use the modern era of 1958–2008 for observations.

3. Results

3.1. AWP Climatology and Annual Cycle

[5] The AWP climatology as determined by the mean climatology of the JAS SST ($\geq 28.5^{\circ}\text{C}$) is shown from

observations in Figure S1a and from the SH at lead-time 0 (for example) in Figure S1b. At lead-time 0, the SH integrations show reasonable agreement with observations in terms of spatial extent. This feature of the model is quite encouraging in light of the fact that many of the coupled climate models are unable to even define an AWP [Misra et al., 2009]. However, the CFS displays seasonal errors of over 1°C (0.5°C) in the Gulf of Mexico (the Caribbean Sea and northwest tropical Atlantic). The seasonal AWP evolution in the observations and in the LT integrations is

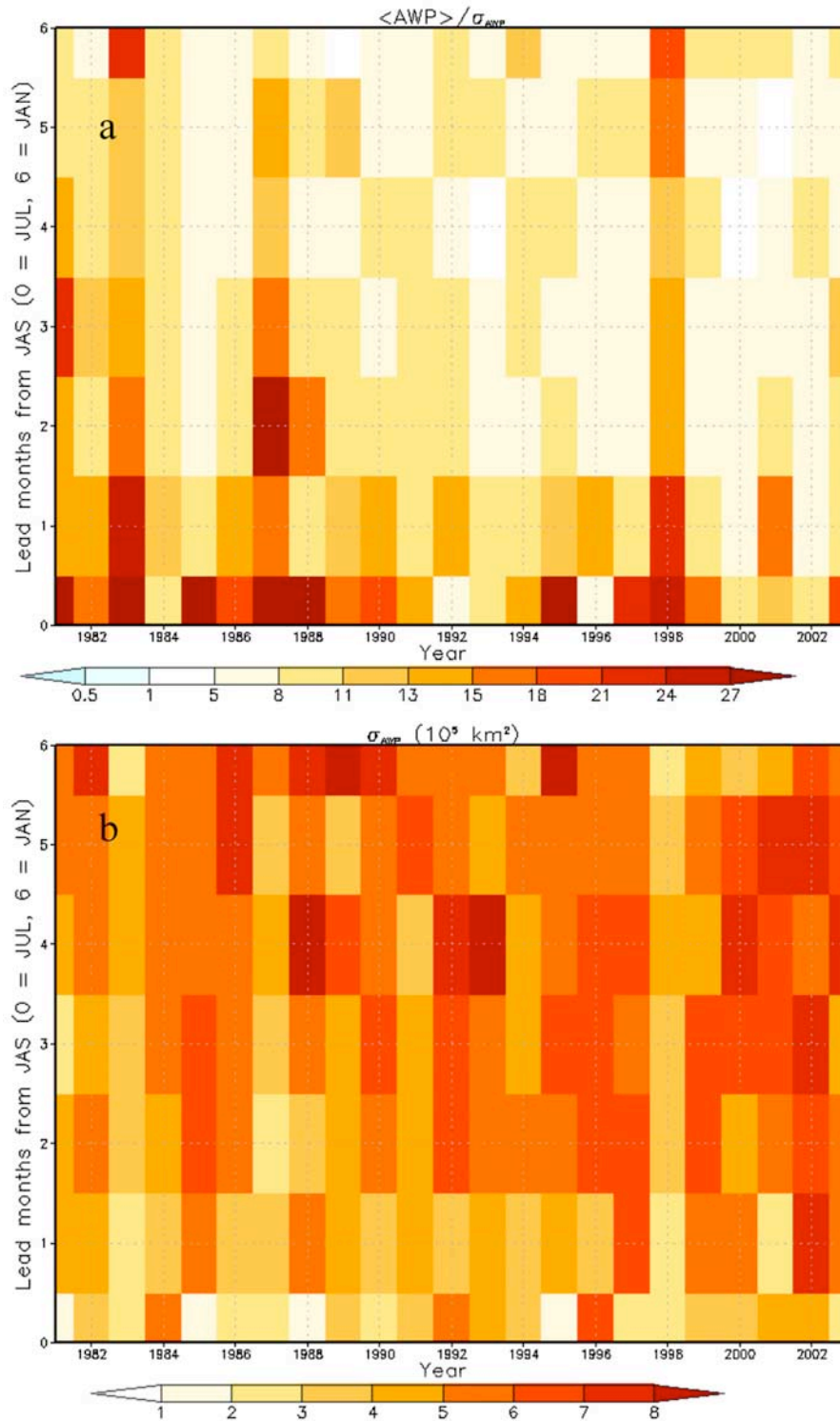


Figure 2. (a) The ratio of the ensemble mean ($\langle AWP \rangle$) of the area of the AWP to its ensemble spread (σ_{AWP}) and (b) the ensemble spread of SH as a function of lead time and year.

comparable (Figure S2). The appearance of the 28.5°C contour in the eastern Pacific in the boreal spring and its extension into the western Atlantic Ocean in the boreal summer is well represented in the NCEP CFS. Likewise, the observed extension of the AWP into the Caribbean Sea in the early boreal autumn and the subsequent demise of the AWP in boreal winter are also simulated in the NCEP CFS.

3.2. Seasonal Errors

[6] The Root Mean Square Error (RMSE) and the Anomaly Correlation Coefficient (ACC) of the mean JAS AWP area as a function of lead time from the CFS SH as a function of lead time are shown in Figures S5a and S5b, respectively. Figures S5a and S5b show that neither RMSE nor ACC shows a systematic linear relation with lead time

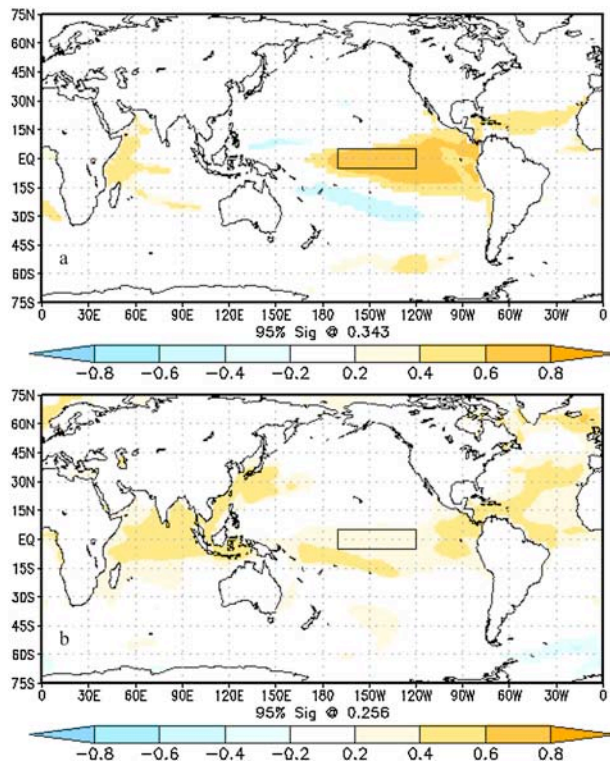


Figure 3. The lead-lag correlation of the JAS seasonal mean area of the AWP with the previous DJF mean global SST from (a) NCEP CFS LT integration and (b) observations [Smith *et al.*, 2008]. Only significant values at 95% confidence interval according to t-test are plotted. The Niño3.4 region is outlined over the central Pacific.

in the CFS SH. Alternatively, the seasonal AWP error in the SH is shown as a function of lead-time and year in Figure 1a. Figure 1a shows that in many years the seasonal AWP error grows with lead-time. Also, in the period from 1997 to 2003, the SH displayed an under representation of the AWP area that is largely unprecedented (Figure 1a). This change in sign of the seasonal errors is, we contend, a result of the Atlantic Multi-decadal Oscillation (AMO) [Kerr, 2000; Enfield *et al.*, 2001] not being properly simulated or initialized in the SH.

[7] The evidence of such a decadal oscillation in the observed SST in the region is clearly evident from Figure S3. Figure S3 indicates that the linear trend from 1950 to 2003 is relatively small compared to the changing slope of the decadal trends from 1950 to 1981 and 1982 to 2003 in the region, which is also confirmed in other studies [Enfield *et al.*, 2001; Kerr, 2000]. The mean JAS SST climatologies for the periods 1982–1996 and 1997–2003 from the observations and the SHs (at 0 lead time, for example) are shown in Figure S4. Clearly, the mean observed SST for the two periods shows significant differences in Figures S4a and S4b. In contrast, the SH shows insignificant differences in the seasonal mean climatology between the two periods (Figures S4c and S4d). The climatological seasonal mean errors of the SH reflect this difference in observations in Figures S4e and S4f, which indicates positive SST bias in the 1982–1996 period compared to the negative bias in the 1997–2003 period. This is consistent with Wang *et al.*

[2008b], who show that the AMO manifestation is also visible in the AWP variations on decadal time scales.

[8] Having shown the evidence for the presence of the decadal variations in the JAS seasonal mean observed SST and its absence in the corresponding SH SST over the AWP region, we now re-compute the errors shown in Figure 1a after passing the observed SST through an 8-year high-pass (4th order Butterworth) filter to remove variability longer than interannual time scales, which is dominated by ENSO time scales (2–7 years; Figure 1b). The signs of the seasonal errors are nearly uniform in Figure 1b, clearly indicating the influence of the observed decadal oscillation on the diagnosis of the AWP seasonal errors of the SH.

3.3. Interannual Variability

[9] A measure of the deterministic signal to noise ratio (defined in the auxiliary material) as a function of lead-time of the SH is shown in Figure S6. It is apparent from Figure S6 that the ratio decreases with lead time, suggesting the growth of the internal variations over the AWP area in the CFS as it moves farther away from the initial time. We have also plotted in Figure 2a the ratio of the ensemble mean of the AWP area to its ensemble spread (standard deviation about the ensemble mean) as a function of lead time and year of the SH. Here it is seen that for a majority of the years, at short lead times (0 and 1) the ratio is relatively larger than at longer lead times. This is consistent with Figure S6. In 1983, 1987 and 1998, this ratio is relatively large at all lead times, indicating the possible influence of the ENSO variations in the eastern equatorial Pacific Ocean. The ensemble spread (noise) about the ensemble mean in Figure 2b clearly indicates that it increases with an increase in lead-time. In 1983, 1987 and 1998, the relative increase of this noise with lead-time is less compared to the other years. In Figures 3a and 3b, the correlations of the JAS seasonal mean AWP area with the previous DJF global SST correlations are shown for the CFS LT integration and observations. The CFS clearly shows the stronger influence of ENSO variations over the AWP region in Figure 3a, which is unsubstantiated in the observations (Figure 3b). Given such an ENSO teleconnection pattern, it is not surprising to observe ENSO's influence on the seasonal predictability of the AWP in the NCEP CFS seasonal hindcasts.

[10] The concept of ensemble integrations for seasonal prediction is not new [Moore and Kleeman, 1996]. In fact, the indeterminate nature of seasonal predictability warrants that sufficient ensemble integrations are performed so that robust probabilistic forecast measures can be computed [Palmer *et al.*, 2000; Kirtman, 2003; Misra, 2004; Saha *et al.*, 2006]. Here, the probabilistic skill is evaluated using the area under the Relative Operating Characteristic (ROC) curves (explained in the auxiliary material) [Graham *et al.*, 2000; Hanley and McNeil, 1982]. Owing to decadal variations in the seasonal errors, we compute the ROC curves (Figure 4) for SH covering the whole period from 1981–2003 and for the period 1981–1996 (when the decadal variations of the observed SST over the AWP area are in one phase). In Figure 4a, it is apparent that the skill of predicting the AWP area in the SH is rather disappointing, when considering the whole period of 1981–2003. However when using the truncated period of the SH, Figure 4b

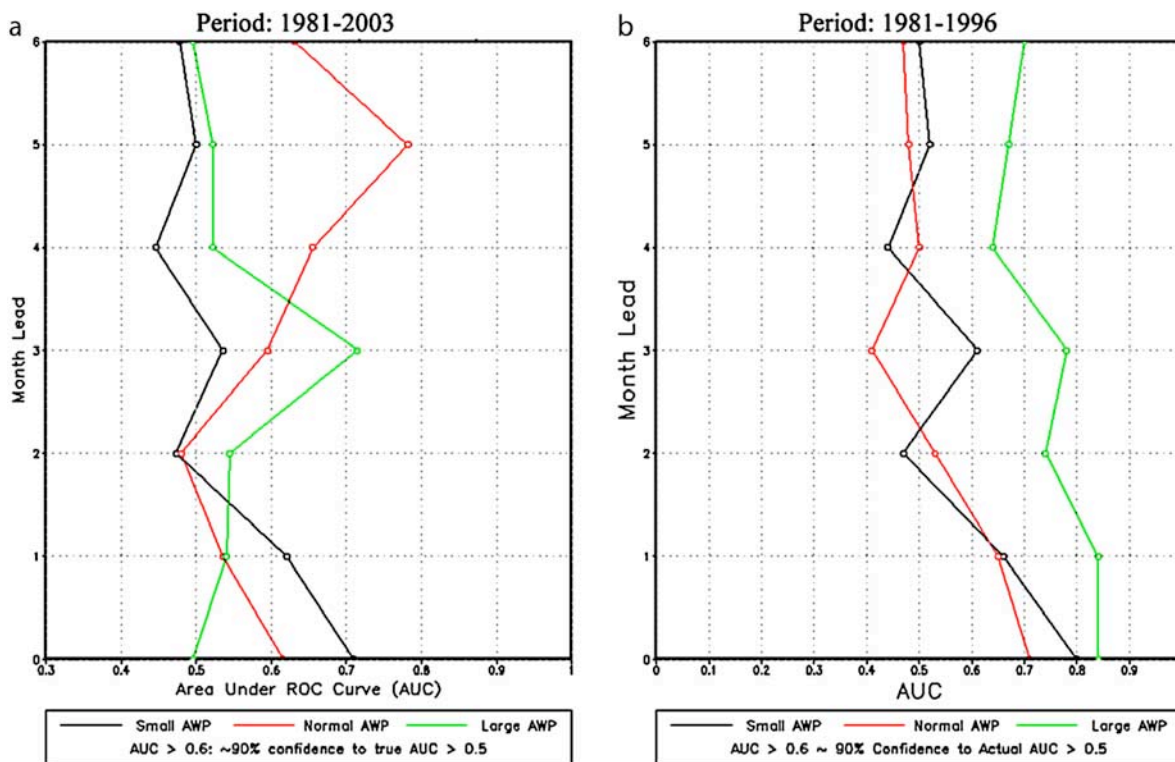


Figure 4. The area under the relative operating curve (AUC) for (a) the full hindcast period of 1981–2003 and (b) the period 1981–1996 when the decadal variations of observed SST in the AWP region are in one phase (see Figure S4).

shows that the SH has skill (when area exceeds 0.6 for 90% confidence interval) in predicting the large AWP events (defined in the upper tercile) at all lead times. (Anomalous AWP events including large, small, and normal are explained in the auxiliary material.) For small (defined in the lowest tercile) and normal (in between the upper and lower tercile) AWP events, the significant probabilistic skill at 90% confidence level is restricted to lead times of 0 and 1. This yet again shows that the observed robust decadal variation in the AWP area is detrimental to the CFS SH prediction skill of AWP.

4. Conclusions

[11] The NCEP CFS Seasonal Hindcasts (SH) produce a reasonable climatology of the AWP. The SH lack the robust decadal SST variations observed over the AWP region. This points to a possible issue with model error (possibly with the ocean model dynamics) and/or the inadequacy of the ocean initialization procedure to capture the decadal variations in the sub-surface oceans. In majority of the years of the SH, the ensemble spread of the area of the AWP increases with lead time, with a consequent decrease in signal to noise ratio with lead time. However such linear relationship of the seasonal errors of the area of AWP with lead time is found lacking in the SH. In contrast, the signal to noise ratio decreases with lead time, which is most likely a result of the noise (ensemble spread) increasing with the lead time. However, in some of the major ENSO years, the SH displays significant increases in signal to noise ratio at all lead times relative to other years. This seems to suggest that large ENSO events, as seen in 1998, 1987, and 1983,

may have some influence on the predictability of the AWP events in the NCEP CFS. It is seen that the NCEP CFS displays erroneously stronger influence of ENSO on the interannual variation of the AWP area. The probabilistic skill as measured by the area under the ROC curve clearly indicates the absence of any useful skill in predicting the modulation of the AWP area in the SH. However, it is found that when we examine a truncated period of the SH (1981–1996 when the observed SST is one phase of the prevalent decadal variation) then some useful skill for the large AWP events (that occur in the upper tercile) at all lead times of the SH is noticed. But in this truncated period of the SH the significant probabilistic skill for the small AWP events (that occur in the lower tercile) and for normal AWP events (that occur in between the lower and upper terciles) is restricted to lead times of 0 and 1 month. These results clearly suggest the importance of decadal variations of Atlantic SST and its lack of adequate representation in the NCEP CFS SH that reflects in its prediction skill of the AWP modulation at interannual scales.

[12] **Acknowledgments.** I would like to acknowledge the expert guidance of Meredith Field of COAPS for her editorial corrections on an earlier version of the manuscript. This research was supported by NOAA grant NA07OAR4310221 and FSU FYAP research grant.

References

- Enfield, D. B., A. M. Mestas-Nuñez, and P. J. Trimble (2001), The Atlantic multidecadal oscillation and its relation to rainfall and river flows in the continental U.S., *Geophys. Res. Lett.*, *28*, 2077–2080, doi:10.1029/2000GL012745.
- Graham, R. J., A. D. L. Evans, K. R. Mylne, M. S. J. Harrison, and K. B. Robertson (2000), An assessment of seasonal predictability using atmo-

- spheric general circulation models, *Q. J. R. Meteorol. Soc.*, *126*, 2211–2240, doi:10.1256/smsqj.56711.
- Hanley, J. A., and B. J. McNeil (1982), The meaning and use of the area under a receiver operating characteristic curve, *Diagn. Radiol.*, *143*, 29–36.
- Kang, I.-S., J.-Y. Lee, and C.-K. Park (2004), Potential predictability of summer mean precipitation in a dynamical seasonal prediction system with systematic error correction, *J. Clim.*, *17*, 834–844, doi:10.1175/1520-0442(2004)017<0834:PPOSMP>2.0.CO;2.
- Kerr, R. A. (2000), A North Atlantic climate pacemaker for the centuries, *Science*, *288*, 1984–1986, doi:10.1126/science.288.5473.1984.
- Kirtman, B. P. (2003), The COLA anomaly coupled model: Ensemble ENSO prediction, *Mon. Weather Rev.*, *131*, 2324–2341, doi:10.1175/1520-0493(2003)131<2324:TCACME>2.0.CO;2.
- Misra, V. (2004), An evaluation of the predictability of austral summer season precipitation over South America, *J. Clim.*, *17*, 1161–1175, doi:10.1175/1520-0442(2004)017<1161:AEOTPO>2.0.CO;2.
- Misra, V., S. Chan, R. Wu, and E. Chassignet (2009), Air-sea interaction over the Atlantic Warm Pool, *Geophys. Res. Lett.*, *36*, L15702, doi:10.1029/2009GL038737.
- Moore, A. M., and R. Kleeman (1996), The dynamics of error growth and predictability in a coupled model of ENSO, *Q. J. R. Meteorol. Soc.*, *122*, 1405–1446, doi:10.1002/qj.49712253409.
- Palmer, T. N., C. Brankovic, and D. S. Richardson (2000), A probability and decision model analysis of PROVOST seasonal multi-model ensemble integrations, *Q. J. R. Meteorol. Soc.*, *126*, 2013–2034, doi:10.1256/smsqj.56702.
- Saha, S., et al. (2006), The climate forecast system at NCEP, *J. Clim.*, *19*, 3483–3517, doi:10.1175/JCLI3812.1.
- Smith, T. M., R. W. Reynolds, T. C. Peterson, and J. Lawrimore (2008), Improvements to NOAA's historical merged land-ocean surface temperature analysis (1880–2006), *J. Clim.*, *21*, 2283–2296, doi:10.1175/2007JCLI2100.1.
- Wang, C., and D. B. Enfield (2001), The tropical Western Hemisphere Warm Pool, *Geophys. Res. Lett.*, *28*, 1635–1638, doi:10.1029/2000GL011763.
- Wang, C., and D. B. Enfield (2003), A further study of the tropical Western Hemisphere Warm Pool, *J. Clim.*, *6*, 1476–1493.
- Wang, C., D. B. Enfield, S.-K. Lee, and C. W. Landsea (2006), Influences of the Atlantic Warm Pool on Western Hemisphere summer rainfall and Atlantic hurricanes, *J. Clim.*, *19*, 3011–3028, doi:10.1175/JCLI3770.1.
- Wang, C., S.-K. Lee, and D. B. Enfield (2008a), Climate response to anomalously large and small Atlantic warm pools during the summer, *J. Clim.*, *21*, 2437–2450, doi:10.1175/2007JCLI2029.1.
- Wang, C., S.-K. Lee, and D. B. Enfield (2008b), Atlantic Warm Pool acting as a link between Atlantic Multidecadal Oscillation and Atlantic tropical cyclone activity, *Geochem. Geophys. Geosyst.*, *9*, Q05V03, doi:10.1029/2007GC001809.

S. Chan and V. Misra, Department of Meteorology, Florida State University, Tallahassee, 404 Love Building, 1017 Academic Way, FL 32306, USA. (vmisra@fsu.edu)

Signal to Noise Ratio

The Signal to Noise Ratio (SNR) for a variable x is computed following Shukla et al. (2000):

$$\sigma_{noise}^2 = \frac{1}{N(M-1)} \sum_{i=1}^N \sum_{j=1}^M (x_{ij} - \bar{x}_i)^2$$

where, x_{ij} represents the climate variable for the i^{th} year of N total years and j^{th} ensemble member of M total ensemble members and \bar{x}_i is the ensemble mean for the i^{th} year.

Similarly, the variance from the signal is given by:

$$\sigma_{signal}^2 = \sigma_{EM}^2 - \frac{1}{m} \sigma_{noise}^2$$

where, the variance of the ensemble mean (σ_{EM}^2) is

$$\sigma_{EM}^2 = \frac{1}{(N-1)} \sum_{i=1}^N (\bar{x}_i - \bar{\bar{x}})^2$$

where, the ensemble mean (\bar{x}_i) for the i^{th} year is given by:

$$\bar{x}_i = \frac{1}{M} \sum_{j=1}^M x_{ij} \text{ and}$$

the climatological mean ($\bar{\bar{x}}$) is given by

$$\bar{\bar{x}} = \frac{1}{NM} \sum_{i=1}^N \sum_{j=1}^M x_{ij}$$

Then,

$$SNR = \frac{\sigma_{signal}^2}{\sigma_{noise}^2}$$

Brief outline of the NCEP CFS LT integration:

The CFS LT integration are 32 years long with 4 ensemble members conducted at the same resolution as the SH i.e., T62 horizontal resolution and 64 levels. These runs follow from Wang et al. (2005) and the documentation of the data from this integration is available at <http://cfs.ncep.noaa.gov/menu/doc/>.

Relative operating characteristic curve:

The ROC curve is based on a contingency table that is developed for each event that is defined. In the paper we define three events that correspond to large, normal and small AWP events. These three categories correspond to lower, middle, and upper tercile of the ranked time series based on the area of the Atlantic Warm Pool computed separately for observations and the NCEP CFS Seasonal Hindcasts (SH). Since robust decadal SST variations are detected in the observations over the AWP region, we limit the ROC calculations from 1981-1996 when the seasonal errors of the AWP in the NCEP CFS SH have a uniform positive sign at all lead times after which, the sign uniformly changes to negative sign. The contingency table is defined below.

Table A1: Contingency table for ROC curves

Is the event observed?	Does ensemble probability for the event exceed threshold X?	
	<i>Yes</i>	<i>No</i>
<i>Yes</i>	Hit (H)	Miss (M)
<i>No</i>	False Alarm (FA)	Correct Rejection (CR)

ROC curves are obtained by plotting hit rates (HR) against false alarm rates (FAR). They are defined as follows:

$$HR = \frac{H}{[H + m]}$$

and

$$FAR = \frac{FA}{[FA + CR]}$$

Then we apply the trapezoidal rule to compute the Area Under the (ROC) Curve (AUC).

Defining anomalous AWP events

These anomalous AWP events are defined to conduct the probabilistic skill analysis of the NCEP CFS SH. The observed time series of the mean JAS AWP area over the period of 1981-2003 is sorted and ranked. We then define small AWP for the lowest tercile. Similarly the large AWP is defined for the upper tercile while the normal AWP is defined for the tercile between the small and large AWP. The occurrence of the anomalous AWP events in the observed time series is shown in Fig. A7. A similar classification is made for the CFS SH.

References:

Shukla, J., and co-authors, 2000: Dynamical Seasonal Prediction. *Bull. Amer. Soc.*, **81**, 2593-2606.

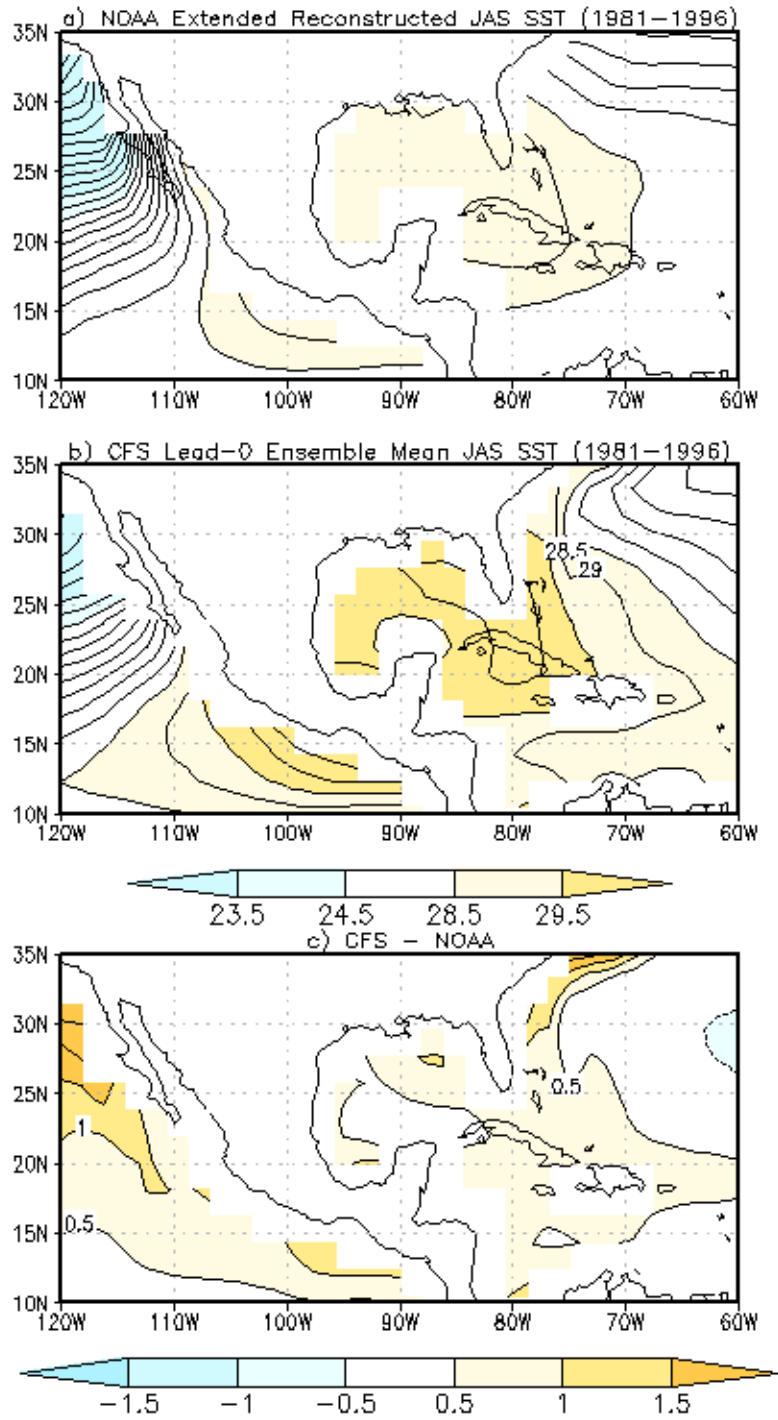


Fig. A1: The climatological July-August-September (JAS) mean SST from a) observations, b) SH at lead time 0 (computed over the time period from 1981-1996), and c) difference between b and c.

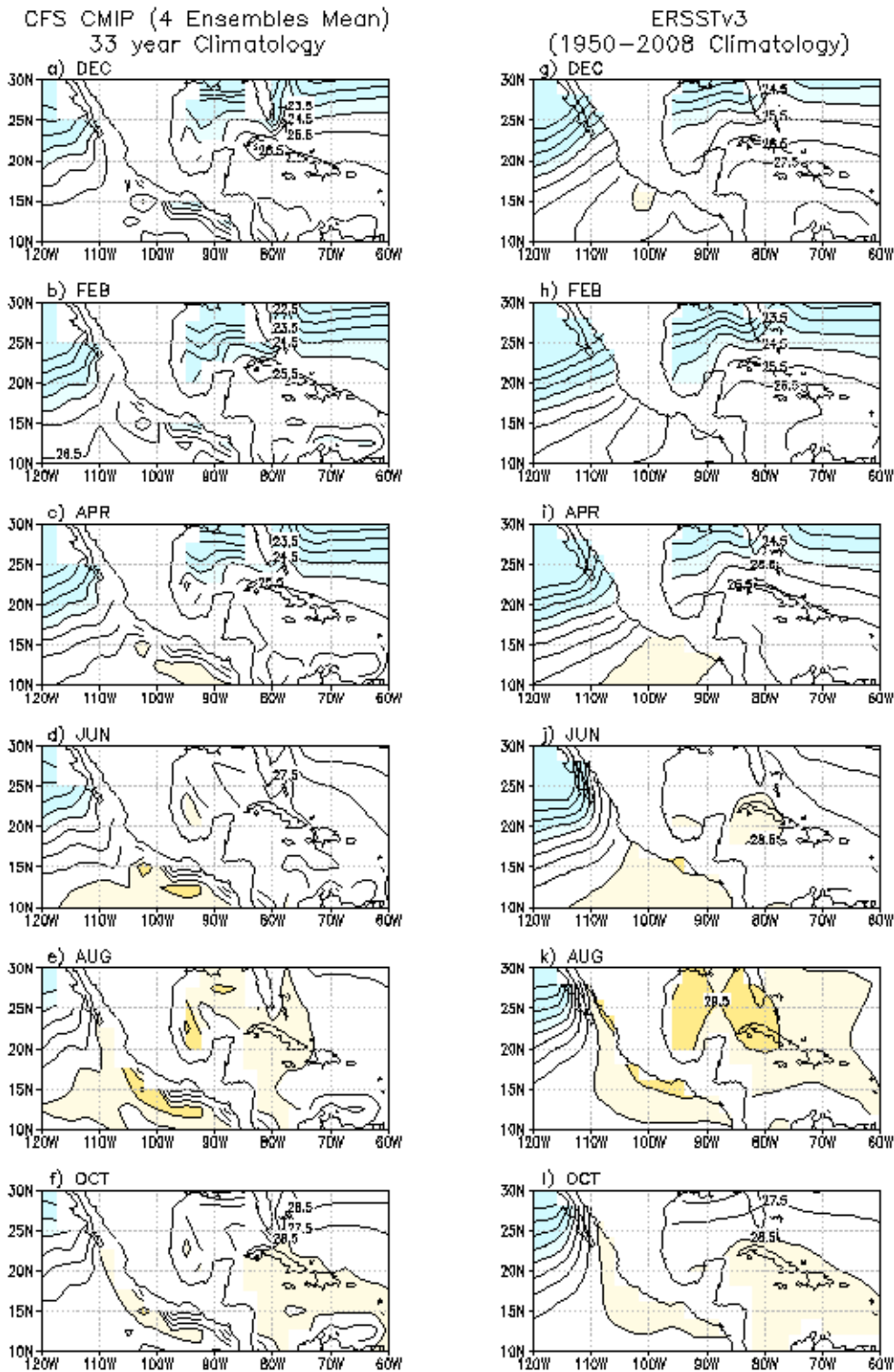


Figure A2: The monthly mean climatology at intervals of two months from the a, b, c, d, e, f) NCEP CFS multi-decadal integrations (CMIP) averaged over four ensemble members and g, h, i, j, k, l) observations.

NOAA Extended Reconstructed SST Version 3 (ERSSTv3)
JAS Trend per Decade (K/10years)

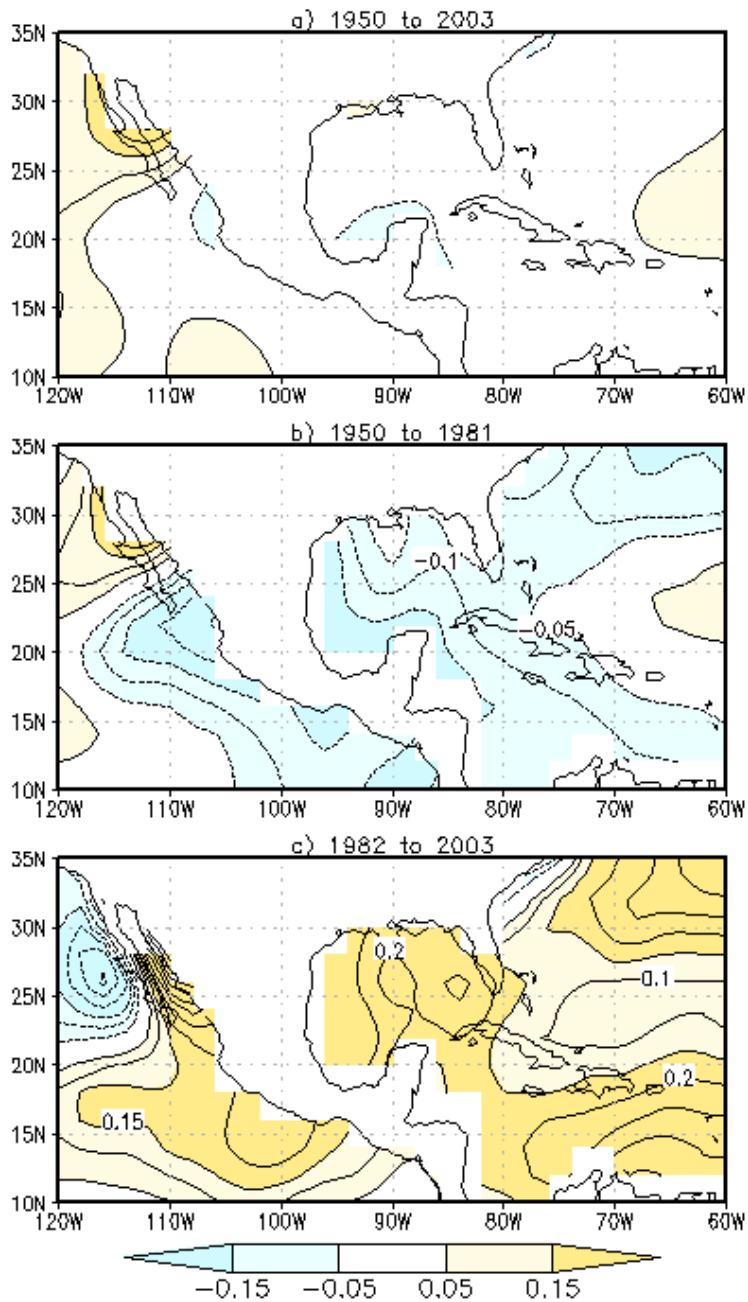


Figure A3: The observed linear trend (per decade) in the July-August September SST over the period of a) 1950-2003, b) 1950-1981, and c) 1982-2003.

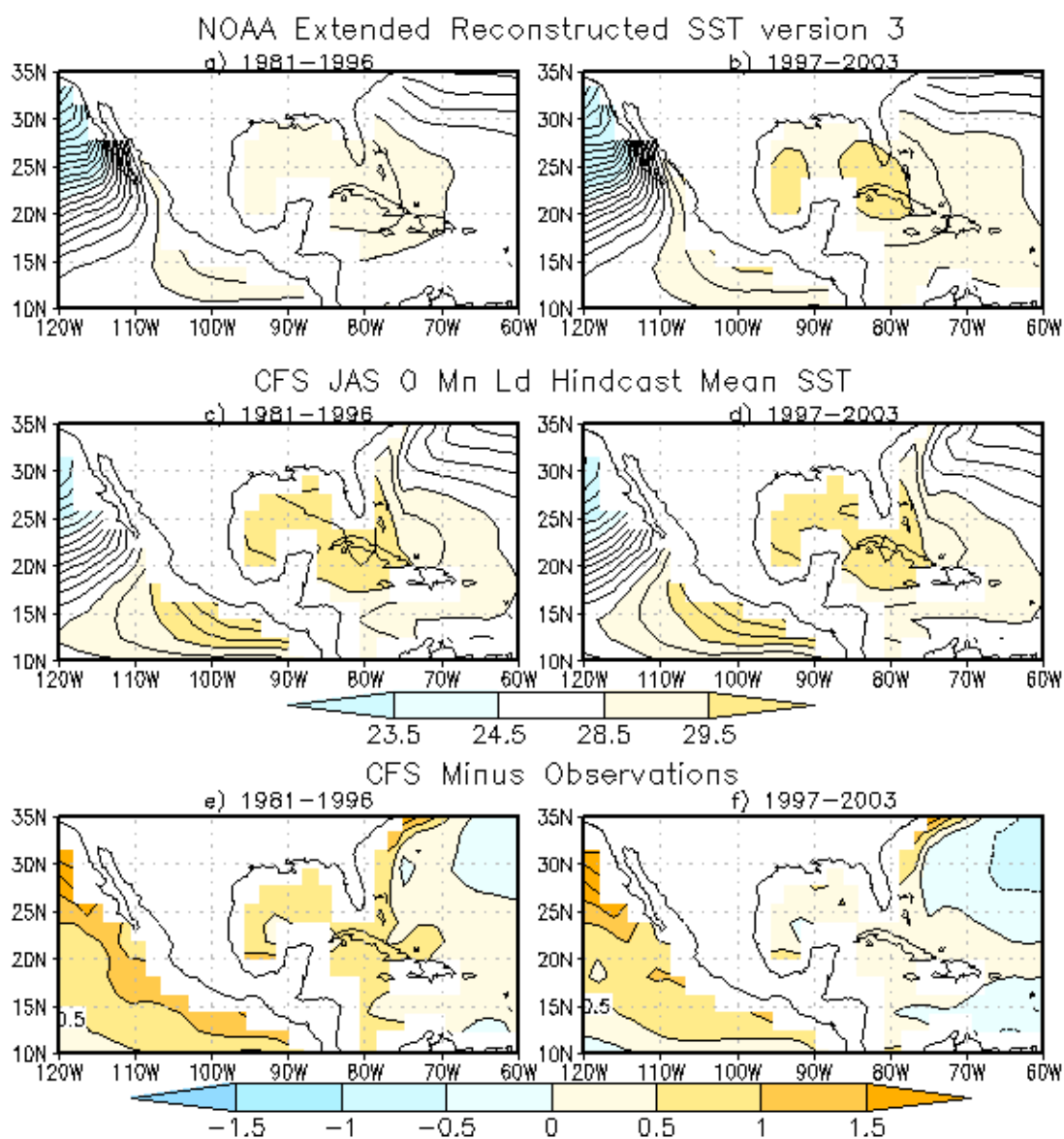


Figure A4: Climatological July-August-September (JAS) seasonal mean SST from observations computed over the period of a) 1982-1996, and b) 1997-2003. Similarly, climatological JAS seasonal mean SST from the SH at 0 lead time computed over a period of c) 1982-1996, and d) 1997-2003. Climatological JAS seasonal mean SH errors computed over a period of e) 1982-1996, and f) 1997-2003.

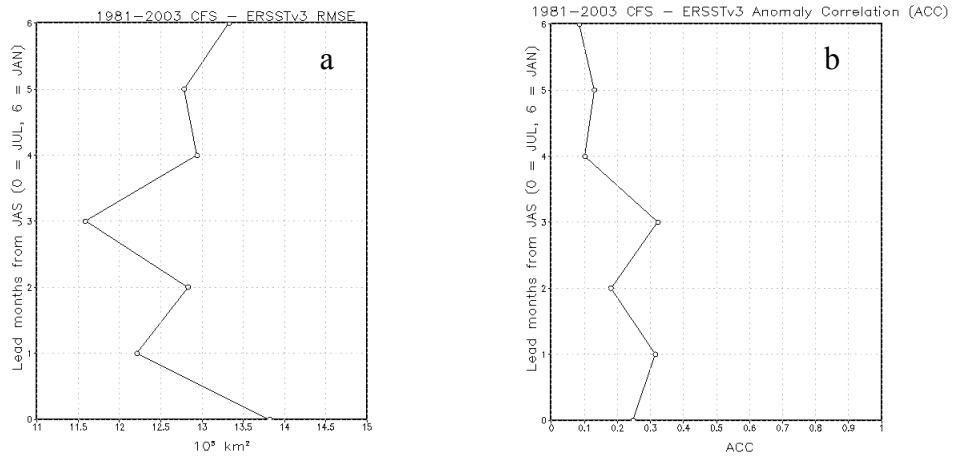


Figure A5: a) Root Mean Square Error (RMSE) and b) Anomaly correlation coefficient (ACC) of the NCEP CFS seasonal hindcasts as a function of lead time covering a period of 1981-2003 .

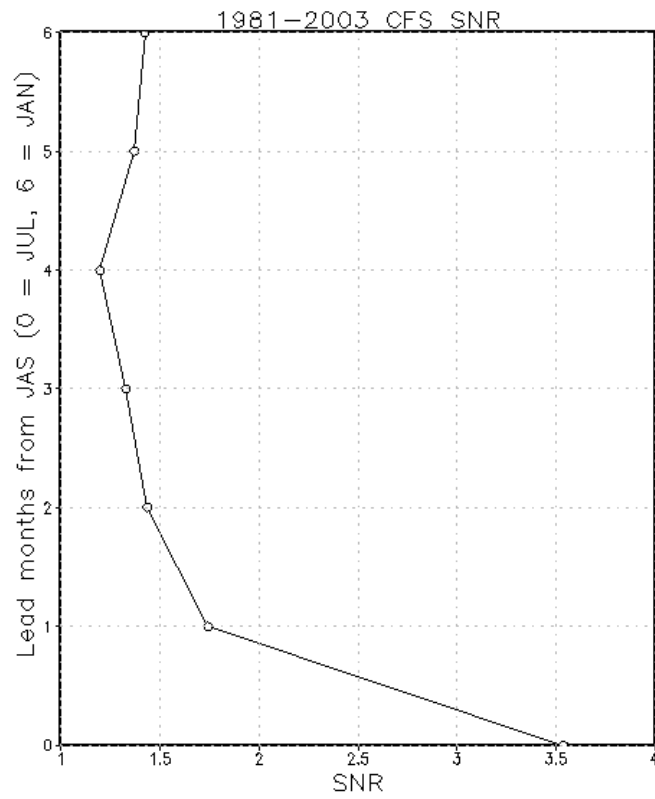


Figure A6: The Signal to Noise Ratio (SNR) of the NCEP CFS seasonal hindcasts for the AWP area as a function of lead time covering a period of 1981-2003 .

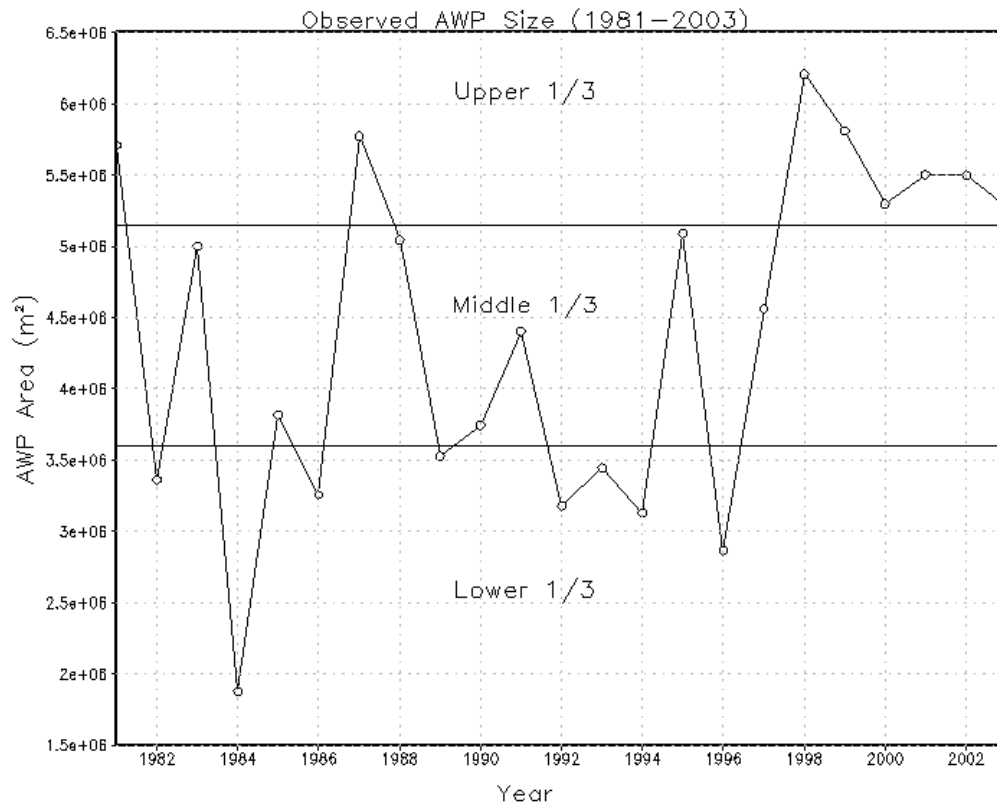


Figure A7: The area of the AWP from observations over a period of 1981-2003, showing the years when anomalously small (lower 1/3), large (upper 1/3) and normal AWP events occur.